step) used by new types of algorithms. (4) Aside from the input and output lines no further means are necessary for the logic operation, for example, additional magnetic fields, switching thresholds, or voltages. (5) The switching frequency of magnetic films can be pushed to several GHz, in principle allowing fast operation[11]. (6) Since only short current pulses are required to rotate the magnetization, the energy consumption is further reduced. (7) The size of an MRAM cell—commercially available in 2004 (ref. 12)—can easily be scaled down to less than 100 nm (refs 13, 14) to further increase the integration density. (8) Our approach a priori does not necessarily require semiconductors to fabricate a logic gate. (9) The run-time programmability will increase the computational efficiency.

Our new approach has the potential to induce a paradigm shift from transistor-based logic to magneto-logic, where the programmable functionality and non-volatility are as important as miniaturization and clock speed. □

Received 12 February; accepted 1 September 2003; doi:10.1038/nature02014.

1. Prinz, G. A. Magnetoelectronics. *Science* **282,** 1660–1663 (1998).
2. Sidhu, R. P. S., Mei, A. & Prasanna, V. K. in *Field-programmable Logic and Applications* (eds Lysaght, P., Irvine, J. & Hartenstein, R. W.) 301–312 (Lecture Notes in Computer Science 1673, Springer, Berlin, 1999.
3. Parkin, S. S. P. *et al.* Exchange-biased magnetic tunnel junctions and application to nonvolatile magnetic random access memory. *J. Appl. Phys.* **85,** 5828–5833 (1999).
4. Grünberg, P. Layered magnetic structures: history, highlights, applications. *Phys. Today* **54,** 31–37 (2001).
5. Baibich, B. N. *et al.* Giant magnetoresistance of (001)Fe/(001)Cr magnetic superlattices. *Phys. Rev. Lett.* **61,** 2472–2475 (1988).
6. Binasch, G., Grünberg, P., Saurenbach, F. & Zinn, W. Enhanced magnetoresistance in layered magnetic structures with antiferromagnetic interlayer exchange. *Phys. Rev. B* **39,** 4828–4830 (1989).
7. Moodera, J. S., Kinder, L. R., Wong, T. M. & Meservey, R. Large magnetoresistance at room temperature in ferromagnetic thin film tunnel junctions. *Phys. Rev. Lett.* **74,** 3273–3276 (1995).
8. Black, W. C. Jr & Das, B. Programmable logic using giant-magnetoresistance and spin-dependent tunneling devices. *J. Appl. Phys.* **87,** 6674–6679 (2000).
9. Richter, R. *et al.* Field programmable spin-logic based on magnetic tunneling elements. *J. Magn. Magn. Mater.* **240,** 127–129 (2002).
10. Martin, A. J. *Proceedings of SSGRR 2000, International Conference on Advances in Infrastructure for Electronic Business, Science, and Education on the Internet*; at ⟨http://www.ssgrr.it/en/ssgrr2000/papers/185.pdf⟩ (2000).
11. Gerrits, Th., van den Berg, H. A. M., Hohlfeld, J., Bär, L. & Rasing, Th. Ultrafast precessional magnetization reversal by picosecond magnetic field pulse shaping. *Nature* **418,** 509–511 (2002).
12. Motorola Inc. Press release. IEEE International Solid State Circuits Conference (San Francisco, June 2001); at ⟨http://www.motorola.com/mot/document/content/0,1028,372,00.doc⟩ (2000).
13. Goronkin, H., von Allmen, P., Tsui, R. K. & Zhu, T. X. *Nanostructure Science and Technology* (eds Siegel, R. W., Hu, E. & Roco, M. C.) 67–92 (National Science and Technology Council (NSTC) Committee on Technology and The Interagency Working Group on NanoScience, Engineering and Technology (IWGN), 1999); at ⟨http://www.wtec.org/loyola/nano/05_01.htm⟩ (1999). Copyright is held by: WTEC, Loyola College (Maryland).
14. Compañó, R. *Technological Roadmap for European Nanoelectronics* at ⟨ftp://ftp.cordis.lu/pub/ist/docs/fetnidrm.zip⟩ (2000).

Competing interests statement The authors declare that they have no competing financial interests.

Correspondence and requests for materials should be addressed to R.K. (koch@pdi-berlin.de).

Controlling anisotropic nanoparticle growth through plasmon excitation

Rongchao Jin, Y. Charles Cao, Encai Hao, Gabriella S. Métraux, George C. Schatz & Chad A. Mirkin

Department of Chemistry and Institute for Nanotechnology, Northwestern University, Evanston, Illinois 60208, USA

Inorganic nanoparticles exhibit size-dependent properties that are of interest for applications ranging from biosensing[1–5] and catalysis[6] to optics[7] and data storage[8]. They are readily available in a wide variety of discrete compositions and sizes[9–14]. Shape-selective synthesis strategies now also yield shapes other than nanospheres, such as anisotropic metal nanostructures with interesting optical properties[15–23]. Here we demonstrate that the previously described photoinduced method[23] for converting silver nanospheres into triangular silver nanocrystals—so-called nanoprisms—can be extended to synthesize relatively monodisperse nanoprisms with desired edge lengths in the 30–120 nm range. The particle growth process is controlled using dual-beam illumination of the nanoparticles, and appears to be driven by surface plasmon excitations. We find that, depending on the illumination wavelengths chosen, the plasmon excitations lead either to fusion of nanoprisms in an edge-selective manner or to the growth of the nanoprisms until they reach their light-controlled final size.

The photoinduced synthesis of silver (Ag) nanoprisms involves the preparation of a colloidal suspension of Ag spheres (diameter <10 nm), followed by conversion of the spheres to larger prism structures with visible light. In a typical experiment, colloidal Ag nanoparticles passivated with sodium citrate and bis(*p*-sulphonatophenyl)phenylphosphine dihydrate dipotassium (BSPP) (diameter 4.8 ± 1.1 nm, standing solution) were irradiated with a narrow-band light source (using a 150 W xenon lamp with a light output $\sim$12 W) with an optical bandpass filter (centre wavelength 550 nm, width 40 nm) for $\sim$50 h (see Supplementary Information). Transmission electron microscopy (TEM) shows that the colloid formed consists of two different size distributions of nanoprisms (Fig. 1a and inset), with the smaller particles (designated as type 1) and the larger particles (type 2) having average edge lengths of 70 ± 12 nm and 150 ± 16 nm, respectively. These structures tend to form stacks, so that edge-on views allow the precise determination of nanoprism thickness[23]. Although the average edge lengths for the type 1 and type 2 nanoprisms are significantly different, their thicknesses are almost identical (9.8 ± 1.0 nm) (Fig. 1b, c).

The bimodal particle growth process also has been monitored by ultraviolet–visible–near-infrared (UV–vis.–NIR) spectroscopy (Fig. 2a). During the reaction, one sees the disappearance of the plasmon band at $\sim$395 nm (characteristic of the spherical silver particles) and the formation of two new, strong plasmon bands at 680 nm and 1,065 nm that are associated with the type 1 and type 2 nanoprisms, respectively (see below). The band for the type 1 prisms is initially centred at $\lambda_{max} = 680$ nm and gradually blue-shifts to $\lambda_{max} = 640$ nm. This blue-shifting correlates with the tip sharpness of the nanoprism features; rounding is known to lead to blue-shifting[24]. The second strong band at $\lambda_{max} = 1{,}065$ nm is assigned to type 2 particles (see below). In addition to the two strong surface plasmon bands, one can observe two other weak resonances at 340 and 470 nm, respectively (Fig. 2a, spectrum 6). To gain further insight into the optical spectra of the solution with the bimodal particle distribution, we carried out theoretical modelling using a finite-element-based method known as the discrete dipole approximation (DDA)[24–26]. The calculated spectrum shows plasmon bands that reproduce the experimentally observed spectrum (compare Fig. 2b and Fig. 2a, spectrum 6), confirming our peak assignments. The first three peaks in the spectrum of the colloid containing both type 1 and type 2 particles, centred at 340 nm (out-of-plane quadrupole resonance), 470 nm (in-plane quadrupole resonance) and 640 nm (in-plane dipole resonance)[24], result from the type 1 nanoprisms; in the case of the type 2 nanoprisms, only the strong dipole resonance at 1,065 nm is clearly observed. Quadrupole resonances, which occur at 340 nm and 600 nm (weak) in the spectrum of the solution of the type 2 nanoprisms, are overlapped with plasmon bands from the type 1 nanoprisms (Fig. 2b). The time-dependent optical spectra thus suggest that the process is bimodal, rather than unimodal as would be expected in the case of conventional Ostwald ripening[13,14].

The bimodal growth of Ag nanoprisms is not caused by the wavelength dispersity of the excitation beam (550 ± 20 nm). Indeed, when a monochromatic laser beam ($\lambda = 532.8$ nm, the

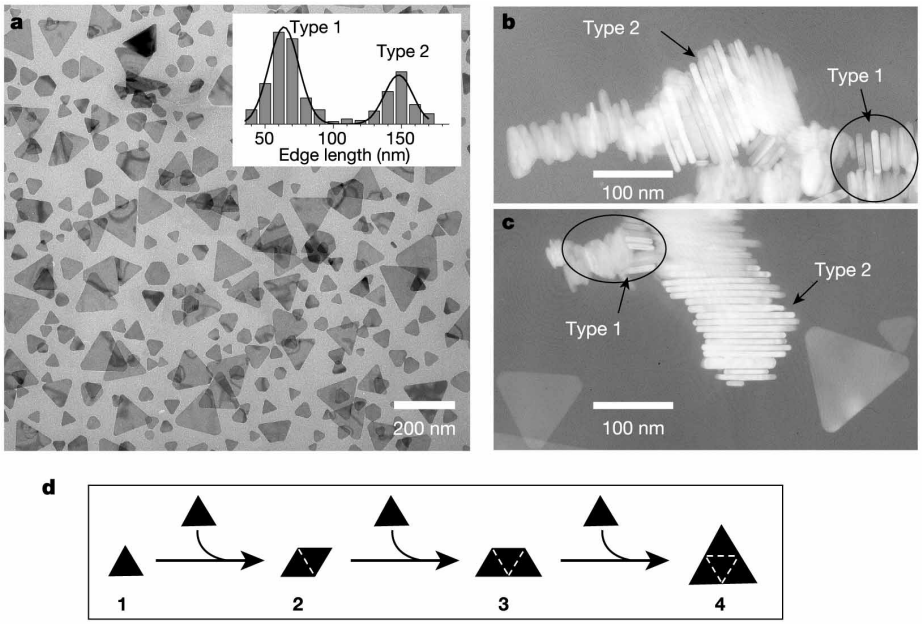

Figure 1 The bimodal growth of Ag nanoprisms. **a**, TEM image of a sample of Ag nanoprisms formed using single-beam excitation (550 ± 20 nm); inset, histograms used to characterize the size distribution as bimodal. **b**, **c**, TEM images of nanoprism stacks showing that nanoprisms have nearly identical thicknesses (9.8 ± 1.0 nm). **d**, Schematic diagram of the proposed light-induced fusion growth of Ag nanoprisms.

second harmonic of a Nd:YAG laser, CW, light output ~0.2 W) is used to photolyse the Ag colloids, bimodal growth is still observed (see Supplementary Information). The bimodal growth was also observed with other excitation wavelengths (500–700 nm). Additional experiments where the surfactant BSPP was absent from the reaction mixture and initial Ag colloid yielded comparable results, demonstrating that BSPP is not critical for effecting the bimodal growth process and nanoprism formation. In addition, the bimodal growth process was observed for a variety of BSPP:sodium citrate ratios (investigated molar ratios ranged from 0:1 to 1:1, with sodium citrate fixed at 0.3 mM) and with different silver salt precursors ($AgNO_3$, CH_3CO_2Ag, $AgClO_4$ and Ag_2SO_4).

We propose that the observed bimodal growth process occurs through an edge-selective particle fusion mechanism, with four type 1 nanoprisms coming together in step-wise fashion to form a type 2 nanoprism (Fig. 1d). The following observations are consistent with this mechanism. First, bimodal growth results in type 1 and type 2 prisms where four of the former prisms can fit together to form a prism with dimensions (cumulative edge length, 140 ± 17 nm) that compare well with the latter (150 ± 16 nm) (Fig. 1). Second, edge-selective growth occurs with no apparent change in nanostructure thickness in going from the type 1 to type 2

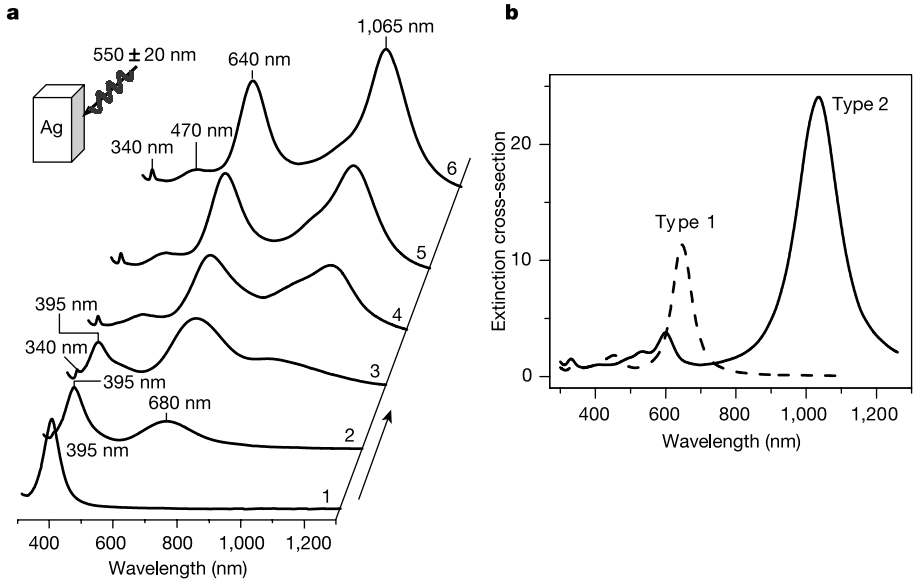

Figure 2 The optical spectra of Ag nanoprisms. **a**, Time evolution of UV–vis.–NIR spectra of a Ag colloid (4.8 ± 1.1 nm spheres) under single-beam excitation (550 ± 20 nm). Spectrum 1, initial colloid; 2, after 10 h; 3, after 15 h; 4, after 19 h; 5, after 24 h; and 6, after 55 h. **b**, Theoretical modelling of the optical spectra of two different-sized nanoprisms (model parameters: edge length of type 1, 70 nm, type 2, 150 nm; thickness, 10 nm). Note that the tip truncation of nanoprisms, which leads to a blueshift of the dipole resonance from 770 to 640 nm, has been taken into account in the modelling.

prisms. Third, detailed time-dependent UV–vis.–NIR measurements show that the onset of the growth of the band at 1,065 nm (assigned to type 2) is significantly delayed in comparison with the growth of the band at 640 nm (assigned to type 1) (Fig. 2a). This indicates that the fusion of nanoprisms occurs only after type 1 nanoprisms have accumulated. Fourth, a small population of dimer **2** and trimer **3** intermediates (Fig. 1d) is observed during the early stages of type 2 particle growth (see Supplementary Information).

We also performed electrodynamics calculations on the optical properties of possible intermediate species involved in the fusion growth process. The results show that intermediates **2** and **3** have dipole plasmon excitations close to 600 and 1,065 nm (see Supplementary Information). Type 1 particles and the intermediates **2** and **3** can thus all absorb light at 600 nm, which can lead to the excited state needed for particle fusion to occur. However, the type 2 particles do not show dipole plasmon excitation explaining why they represent the end of the particle growth path. Note in this context that removal of surface ligands has, in the case of CdTe (ref. 27) and PbSe (C. B. Murray, personal communication), resulted in the fusion of spherical particles into nanowire structures; similar examples involving spherical particle fusion have also been reported[28].

At first glance, the observed bimodal growth appears to contradict previous results in which unimodal nanoprism growth was observed when visible light (white) from a conventional fluorescent tube was used as the excitation source[23]. By careful analysis of the optical properties of these nanostructures and the effects of photolysis on them, we have identified a type of surface plasmon cooperativity in the photochemistry of Ag nanoprisms. To demonstrate this cooperative effect on nanoprism growth, we excited a solution of Ag nanoparticles (4.8 ± 1.1 nm) at two wavelengths, 550 ± 20 nm (primary) and 450 ± 5 nm (secondary) (I_{550}:I_{450} = 2:1, Fig. 3a). The 450-nm wavelength was selected to excite the quadrupole plasmon of the type 1 prisms. Double-beam excitation at these wavelengths inhibits the formation of type 2 nanoprisms and results in exclusive formation of the smaller type 1 nanoprisms (72 ± 8 nm), as evidenced by UV–vis.–NIR spectra and TEM analysis (Fig. 3b, spectrum 4, and Fig. 3e). We further investigated the effect of varying the wavelength of the secondary beam and found that a 550-nm/340-nm coupled beam, in which the 340-nm light coincides with the out-of-plane quadrupole plasmon of the type 1 nanoprisms, also can inhibit the formation of type 2 nanoprisms and result in unimodal growth. However, in the cases of 550-nm/395-nm, 550-nm/610-nm, and 550-nm/650-nm coupled beams, in which the secondary wavelengths fall within the dipole resonances of the Ag nanospheres (395 nm) and type 1 nanoprisms (610 and 650 nm), respectively, bimodal growth is observed (see Supplementary Information). These data strongly indicate that only secondary wavelengths that can excite quadrupole plasmon modes can inhibit bimodal growth. Indeed, it is this photo-cooperativity that leads to the results observed with a fluorescent tube as the excitation source[23]. The emission spectrum of a fluorescent tube exhibits bands at 546 nm and 440 nm, and has the appropriate intensity ratio (100%:40%) to effect photosynthetic cooperativity and hence unimodal growth. Consistent with this conclusion, when a 550 ± 20 nm band filter is used with a fluorescent tube to effect the photosynthetic conversion, bimodal growth is observed.

This observation of photo-cooperativity provides a way of controlling particle size with light. By supplementing the primary light source (450–700 nm) with a fixed secondary beam (340 nm, corresponding to out-of-plane quadrupole plasmon excitation), we can intentionally effect unimodal growth and generate a solution of nanoprisms of a desired average size. Using this approach, we have been able to synthesize nanoprisms with in-plane dipole plasmon resonances that track with particle size from 30 to 120 nm by using primary excitation wavelengths of 450 ± 20 nm, 490 ± 20 nm, 520 ± 20 nm, 550 ± 20 nm, 650 ± 20 nm and 750 ± 20 nm, respectively (Fig. 3b–f). The average edge lengths of the resulting nanoprisms correlate well with the wavelength of the primary

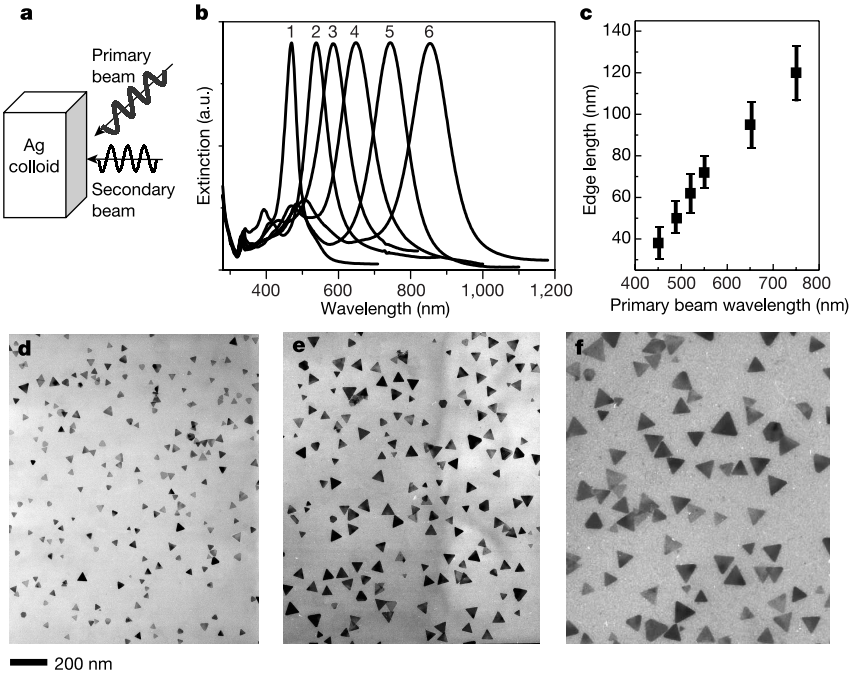

Figure 3 The unimodal growth of nanoprisms. **a**, Schematic diagram of dual-beam excitation. **b**, The optical spectra (normalized) for six different-sized nanoprisms (1–6 edge length: 38 ± 7 nm, 50 ± 7 nm, 62 ± 9 nm, 72 ± 8 nm, 95 ± 11 nm and 120 ± 14 nm) prepared by varying the primary excitation wavelength (central wavelength at 450, 490, 520, 550, 650 and 750 nm, respectively; width, 40 nm) coupled with a secondary wavelength (340 nm; width, 10 nm). **c**, The edge lengths as a function of the primary excitation wavelength. **d**–**f**, TEM images of Ag nanoprisms with average edge lengths of 38 ± 7 nm (**d**), 72 ± 8 nm (**e**) and 120 ± 14 nm (**f**). Scale bar applies to panels **d**–**f**.

excitation source (Fig. 3c), which shows that a longer primary excitation wavelength produces larger particles with in-plane dipole plasmons (the red-most peak in each spectrum) that are red-shifted with respect to the excitation wavelength (Fig. 3b).

Another feature of using wavelength to control particle size is that subsequent addition of Ag spherical particles (4.8 ± 1.1 nm) to the nanoprism colloid does not lead to enlargement of the nanoprisms (see Supplementary Information); instead, the particles added photochemically grow into nanoprisms similar in size to the present ones (as determined by the excitation wavelength). This is in contrast to thermal methods for controlling particle sizes, in which addition of precursors typically leads to larger particles[14]. Note that the wavelength control of particle size is not likely to be a result of photothermal (or optical 'burning') effects; such effects have been invoked in other studies involving intense pulse laser irradiation of metal nanostructures (for example, 10^6 W)[29,30]. The light source used to effect nanoprism conversion is very weak (beam power ≤0.2 W). Indeed, according to the equation $\Delta T = \Delta H/C_p$ (where ΔH is the absorbed photon energy, and C_p is the heat capacity of silver, 0.235 $J K^{-1} g^{-1}$), single 550-nm photon absorption by a type 1 prism can only lead to a negligible increase in temperature (≤0.007 K) (see Supplementary Information). The cumulative experimentally determined temperature increase after 50 h of photolysis (550 ± 20 nm) was less than 10 °C.

Surface plasmons are typically studied as physical properties of metal nanostructures rather than chemical tools that provide control over growth and ultimate particle dimensions. The results reported here provide clear evidence for the importance of plasmon excitation in the Ag nanoprism growth process, both for type 1 particles (which apparently grow from the initially produced colloidal particles to a size that depends on the dipole plasmon wavelength) and for type 2 particles (whose growth also requires dipole plasmon excitation, but is inhibited by quadrupole plasmon excitation). Although a detailed mechanism for these types of conversions remains to be determined, it is possible that plasmon excitation does two things. First, it could redistribute charge on the surfaces of the type 1 nanoprisms to either facilitate (in the case of dipole excitation) or inhibit (in the case of quadrupole excitation) particle–particle fusion. In addition, surface plasmon excitation could facilitate ligand dissociation at the particle edges (as this is where the local fields are the most intense[24]), allowing the type 1 particles to grow through the addition of silver atoms or clusters. Taken together, these results are consistent with a new type of particle size control that is initiated and driven by light, highly cooperative, and surface-plasmon directed. □

Received 28 March; accepted 28 August 2003; doi:10.1038/nature02020.

1. Mirkin, C. A., Letsinger, R. L., Mucic, R. C. & Storhoff, J. J. A DNA-based method for rationally assembling nanoparticles into macroscopic materials. *Nature* **382,** 607–609 (1996).
2. Bruchez, M., Moronne, M., Gin, P., Weiss, S. & Alivisatos, A. P. Semiconductor nanocrystals as fluorescent biological labels. *Science* **281,** 2013–2016 (1998).
3. Han, M., Gao, X., Su, J. Z. & Nie, S. Quantum-dot-tagged microbeads for multiplexed optical coding of biomolecules. *Nature Biotechnol.* **19,** 631–635 (2001).
4. Nicewarner-Peña, S. R. *et al.* Submicrometer metallic barcodes. *Science* **294,** 137–141 (2001).
5. Cao, Y. C., Jin, R. & Mirkin, C. A. Nanoparticles with Raman spectroscopic fingerprints for DNA and RNA detection. *Science* **297,** 1536–1540 (2002).
6. Schmid, G. Large clusters and colloids. Metals in the embryonic state. *Chem. Rev.* **92,** 1709–1727 (1992).
7. Wang, J. F., Gudiksen, M. S., Duan, X. F., Cui, Y. & Lieber, C. M. Highly polarized photoluminescence and photodetection from single indium phosphide nanowires. *Science* **293,** 1455–1457 (2001).
8. Sun, S., Murray, C. B., Weller, D., Folks, L. & Moser, A. Monodisperse FePt nanoparticles and ferromagnetic FePt nanocrystal superlattices. *Science* **287,** 1989–1992 (2000).
9. Nirmal, M. *et al.* Fluorescence intermittency in single cadmium selenide nanocrystals. *Nature* **383,** 802–804 (1996).
10. Henglein, A. Radiolytic preparation of ultrafine colloidal gold particles in aqueous solution: optical spectrum, controlled growth, and some chemical reactions. *Langmuir* **15,** 6738–6744 (1999).
11. Brust, M. & Kiely, C. J. Some recent advances in nanostructure preparation from gold and silver particles: a short topical review. *Colloid Surf. A* **202,** 175–186 (2002).
12. Korgel, B. A. & Fitzmaurice, D. Self-assembly of silver nanocrystals into two-dimensional nanowire arrays. *Adv. Mater.* **10,** 661–665 (1998).
13. Talapin, D. V. *et al.* Dynamic distribution of growth rates within the ensembles of colloidal II–VI and III–V semiconductor nanocrystals as a factor governing their photoluminescence efficiency. *J. Am. Chem. Soc.* **124,** 5782–5790 (2002).
14. Peng, X., Wickham, J. & Alivisatos, A. P. Kinetics of II–VI and III–V colloidal semiconductor nanocrystal growth: "focusing" of size distributions. *J. Am. Chem. Soc.* **120,** 5343–5344 (1998).
15. Chang, S. S., Shih, C. W., Chen, C. D., Lai, W. C. & Wang, C. R. C. The shape transition of gold nanorods. *Langmuir* **15,** 701–709 (1999).
16. Sun, Y. G. & Xia, Y. N. Shape-controlled synthesis of gold and silver nanoparticles. *Science* **298,** 2176–2179 (2002).
17. Maillard, M., Giorgio, S. & Pileni, M. P. Silver nanodisks. *Adv. Mater.* **14,** 1084–1086 (2002).
18. Maillard, M., Giorgio, S. & Pileni, M.-P. Tuning the size of silver nanodisks with similar aspect ratios: synthesis and optical properties. *J. Phys. Chem. B* **107,** 2466–2470 (2003).
19. Pastoriza-Santos, I. & Liz-Marzan, L. M. Synthesis of silver nanoprisms in DMF. *Nano Lett.* **2,** 903–905 (2002).
20. Chen, S. H., Fan, Z. Y. & Carroll, D. L. Silver nanodisks: synthesis, characterization, and self-assembly. *J. Phys. Chem. B* **106,** 10777–10781 (2002).
21. Hao, E. C., Kelly, K. L., Hupp, J. T. & Schatz, G. C. Synthesis of silver nanodisks using polystyrene mesospheres as templates. *J. Am. Chem. Soc.* **124,** 15182–15183 (2002).
22. Sun, Y. & Xia, Y. Triangular nanoplates of silver: synthesis, characterization, and use as sacrificial templates for generating triangular nanorings of gold. *Adv. Mater.* **15,** 695–699 (2003).
23. Jin, R. *et al.* Photoinduced conversion of silver nanospheres to nanoprisms. *Science* **294,** 1901–1903 (2001).
24. Kelly, K. L., Coronado, E., Zhao, L. L. & Schatz, G. C. The optical properties of metal nanoparticles: the influence of size, shape, and dielectric environment. *J. Phys. Chem. B* **107,** 668–677 (2003).
25. Yang, W. H., Schatz, G. C. & Van Duyne, R. P. Discrete dipole approximation for calculating extinction and Raman intensities for small particles with arbitrary shapes. *J. Chem. Phys.* **103,** 869–875 (1995).
26. Draine, B. T. & Flatau, P. J. Discrete-dipole approximation for scattering calculations. *J. Opt. Soc. Am. A* **11,** 1491–1499 (1994).
27. Tang, Z., Kotov, N. A. & Giersig, M. Spontaneous organization of single CdTe nanoparticles into luminescent nanowires. *Science* **297,** 237–240 (2002).
28. Penn, R. L. & Banfield, J. F. Imperfect oriented attachment: dislocation generation in defect-free nanocrystals. *Science* **281,** 969–971 (1998).
29. Link, S., Burda, C., Mohamed, M. B., Nikoobakht, B. & El-Sayed, M. A. Laser photothermal melting and fragmentation of gold nanorods: energy and laser pulse-width dependence. *J. Phys. Chem. B* **103,** 1165–1170 (1999).
30. Kamat, P. V. Photophysical, photochemical and photocatalytic aspects of metal nanoparticles. *J. Phys. Chem. B* **106,** 7729–7744 (2002).

Supplementary Information accompanies the paper on **www.nature.com/nature**.

Acknowledgements We acknowledge the use of a Cary 500 spectrometer in the Keck Biophysics Facility at Northwestern University. C.A.M and G.C.S. thank the AFOSR, ONR, DARPA and NSF for support of this work. R.J. is grateful for the support of the American Chemical Society Cognis Fellowship in Colloid and Surface Chemistry.

Competing interests statement The authors declare that they have no competing financial interests.

Correspondence and requests for materials should be addressed to C.A.M. (camirkin@chem.northwestern.edu) or G.C.S. (schatz@chem.northwestern.edu).

Enantiospecific electrodeposition of a chiral catalyst

Jay A. Switzer, Hiten M. Kothari, Philippe Poizot, Shuji Nakanishi & Eric W. Bohannan

Department of Chemistry and Graduate Center for Materials Research, University of Missouri-Rolla, Rolla, Missouri 65409-1170, USA

Many biomolecules are chiral—they can exist in one of two enantiomeric forms that only differ in that their structures are mirror images of each other. Because only one enantiomer tends to be physiologically active while the other is inactive or even toxic, drug compounds are increasingly produced in an enantiomerically pure form[1] using solution-phase homogeneous catalysts and enzymes. Chiral surfaces offer the possibility of developing heterogeneous enantioselective catalysts that can more readily be separated from the products and reused. In addition, such surfaces might serve as electrochemical sensors for chiral molecules. To date, chiral surfaces have been obtained by adsorbing chiral molecules[2–6] or slicing single crystals so that they exhibit high-index faces[7–13], and some of these surfaces act as enantioselective heterogeneous catalysts[5,6,10]. Here we show that

